Photometry of Lunar Landing Sites Using LROC NAC Images and Hapke Modeling

Ryan N. Clegg[1], Bradley L. Jolliff[1], Mark S. Robinson[2], Bruce W. Hapke[3], Jeffrey B. Plescia[4]

[1]Department of Earth and Planetary Sciences and the McDonnell Center for Space Sciences, Washington University in St. Louis, rclegg@levee.wustl.edu,

[2]School of Earth and Space Exploration, Arizona State University, [3]Department of Geology and Planetary Science, University of Pittsburgh, [4]Johns Hopkins University Applied Physics Laboratory

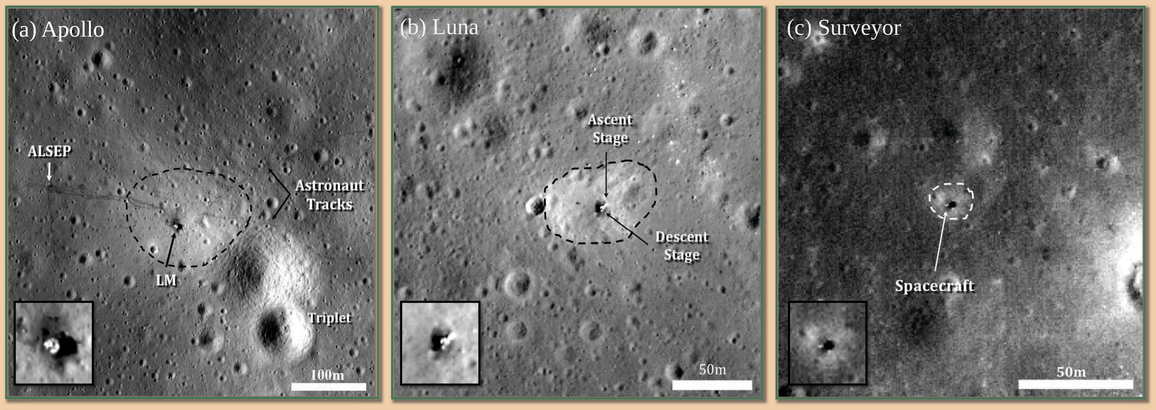

Figure 1: NAC images of the Apollo, Surveyor, and Luna landing sites, cropped to the region around the landers. Dashed lines outline the outer extent of each blast zone (HR-BZ). Insets are zoomed in on the lander. a) Apollo 14, image M11406206L. b) Luna 23, image M174868307R. c) Surveyor 1, image M122495769L.

I. Background

Exhaust from the Apollo, Surveyor, and Luna descent engines interacted with the regolith, creating surface alterations or "blast zones" (BZs). The BZs are visible as regions of different reflectivity surrounding the landers in Lunar Reconnaissance Orbiter Camera (LROC) Narrow Angle Camera (NAC) images (Fig. 1).

- BZs consist of an area of lower reflectance (LR-BZ) that extends up to a few meters from the landers, and a broader halo of higher reflectance (HR-BZ) that extends tens to hundreds of meters from the landers (Fig. 2).
- Aim of study: determine what physical properties of the regolith changed to cause changes in brightness as a result of interaction with rocket exhaust.

II. Hypotheses

We have considered the following to explain reflectance differences:

1) Change in macroscopic roughness (cm to m scale).
2) Redistribution of fine particles within HR-BZs.
3) Removal of mature soil and exposure of less mature soil beneath.
4) Microscopic (nm to μm scale) modification of "fairy-castle" structure, see [1].
5) Compaction of regolith within the more reflective area.
6) Combination of these effects.

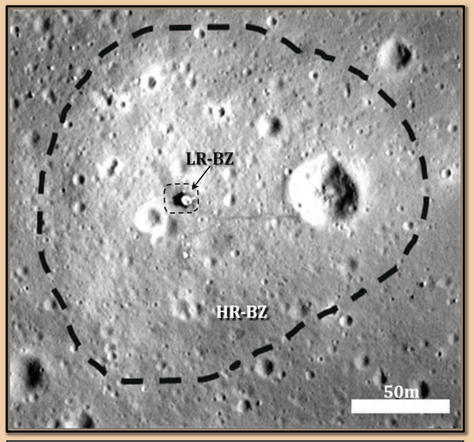

Figure 2: Apollo 11 landing site, with LR-BZ and HR-BZ outlined. Image M150361817R.

III. Methods

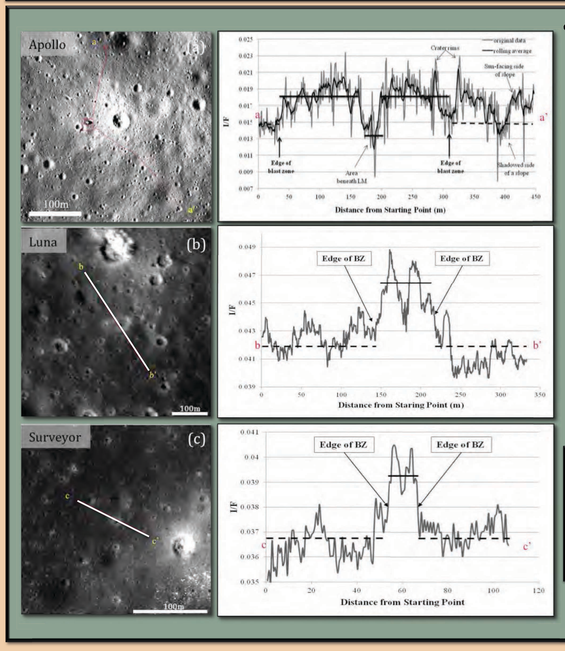

- Phase-ratio images created using NAC images provide enhanced contrast between the disturbed and undisturbed regions [2,3] and are used to measure the spatial extent of BZs. Reflectance profiles give quantitative information on how reflectance (*I/F*) changes within the HR-BZ, the LR-BZ, and background regions. They also provide a measure of spatial extents of the BZs.
- Hapke photometric modeling is used to fit reflectance data over a range of illumination conditions by varying parameters that relate to regolith physical properties [4-7].

Figure 3: Example reflectance profiles. Solid lines indicate average *I/F* within BZ, dashed lines indicate average *I/F* for background. a) Apollo 11, image M150361817R. b) Luna 23, image M106468527R. c) Surveyor 1, image M122495769L.

Photometric Functions

Hapke's Bidirectional Reflectance Equation (from [7])

$$IoF/LS = \frac{w}{4}[p(g) + H(\mu_0, w)H(\mu, w) - 1][1 + B_{C0}B_C(g, h_c)]S(i, e, \theta)$$

$$H(x, w) = \frac{1+2x}{1+2x\sqrt{1-w}}$$

Double Henyey-Greenstein Function:

$$p(g) = \frac{1+c}{2}\frac{1-b^2}{(1-2b\cos g + b^2)^{3/2}} + \frac{1-c}{2}\frac{1-b^2}{(1+2b\cos g + b^2)^{3/2}}$$

Lommel-Seeliger Function (LS):

$$LS = \frac{\mu_0}{(\mu_0 + \mu)} \qquad \mu_0 = \cos(i), \mu = \cos(e)$$

***w* = single scattering albedo**
p(g) = single particle phase function
B_{co} = amplitude of Coherent Backscatter Opposition Effect (CBOE)
B_c = angular shape function of CBOE
h_c = CBOE angular width parameter
S = shadowing parameter
***b* = angular width of forward/ backscattering lobe**
***c* = magnitude of forward/ backscattering lobe**
θ = mean slope angle
i = incidence angle
e = emission angle
g = phase angle

*Bold variables are key parameters

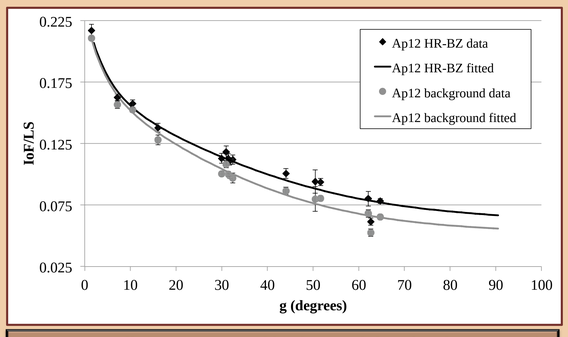

Figure 5: Apollo 12 HR-BZ and background data fitted using Hapke photometric functions.

Table 2: Parameter values used for modeling in Fig. 5

	w	B_{co}	h_c	b	c	θ
HR-BZ	0.305	0.77	0.107	0.35	-0.20	2°
Background	0.305	0.77	0.107	0.40	-0.25	23°

IV. Results

- The average Apollo BZ area is 10× larger than the average Luna BZ, and over 100× larger than the average Surveyor BZ (Table 1).
  - BZ area scales with lander mass and thrust (Table 1).
- Apollo LR-BZs have 15-30% reduction in reflectance at ~30° phase angle compared to the background.
  - Luna and Surveyor LR-BZs are confined to the area below the landers.
- HR-BZ reflectance is 8% higher on average at ~30° phase than in undisturbed areas for all sites.
- HR-BZs are less backscattering than undisturbed areas.
- *I/F* decreases as a function of phase angle [8] (Fig. 4).
  - Separation between BZ and background values becomes proportionally larger at larger phase, consistent with changes in backscattering character.
- *I/F* varies systematically as a function of composition, as expected (Fig. 4b).
- Changing mean slope angle provides for better model fits of the data and reveals HR-BZ is smoother than background - see Fig. 5 and Table 2.
  - Changing *b* and *c* within Henyey-Greenstein Function also provide a better fit and may be related to grain size differences.
- Samples collected within and outside the BZ show no distinguishable trends in particle size and maturity differences that would account for the reflectance phenomena [this work, 9].

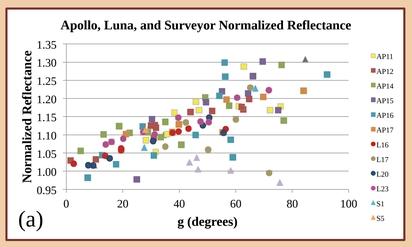

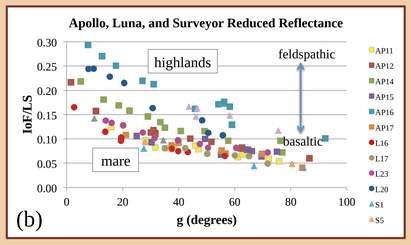

Figure 4: a) HR-BZ reflectance, normalized to background. b) Reduced reflectance (IoF/LS), showing compositional differences between landing sites.

Table 1: Average reflectance values and area measurements for the landing sites. Normalized I/F = IoF(HR-BZ)/IoF(bckgrnd).

Mission	Avg normalized I/F[a]	Avg. elliptical area (m²)	Avg. thrust (kN)
Apollo	1.085	28785	45
Luna[b]	1.089	2380	15-20
Surveyor	1.078	215	0.133-0.472

[a]For images with 30° phase angle
[b]Excluding Luna 24, see [18]

V. Compositional Effects

Published compositional data [10-12] for samples taken within and outside the BZ were compared to modeled *w* values for each site. The correlation between *w* and Al_2O_3 is very good (R^2=0.95) and *w* increases as Al_2O_3 increases. Apollo 16 and Luna 20 landed in the highlands and have the highest Al_2O_3 and plagioclase content, and thus the highest *w*.

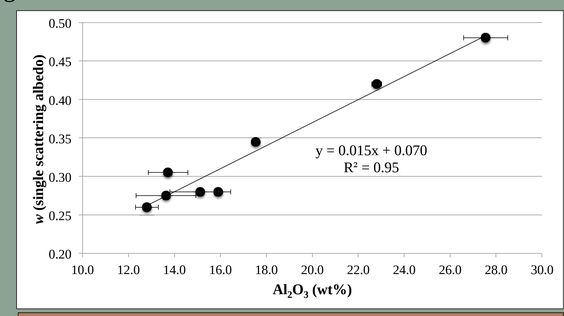

Figure 6: Single scattering albedo values used for modeling as a function of Al_2O_3 content for Apollo and Luna landing sites (excluding Luna 24, see [18]). Errors calculated using data from [9,11].

VI. Conclusions

1) Smoothing and destruction of the fairy-castle structure are possible causes of eflectance increase within the HR-BZs (consistent with [2] and [14]).
2) LR-BZs are darkened by macroscopic disruption of the surface beneath the engine nozzle [15] and by astronaut activity next to the landers, which causes increased roughness and shadowing.
3) Blast effects modeling [15-17] indicates that particles should travel further than the measured extents of HR-BZs, suggesting that redistribution of fine particles within the HR-BZs is not the cause of the reflectance increase.
   - However, photometric modeling does not fully rule out this hypothesis.
4) Exposure of less mature soil is not indicated owing to insignificant excavation by the exhaust plumes [9,14,16].
5) The gas pressure was enough to destroy the fairy-castle structure, but not enough to compact the surface [15].
6) HR-BZ area extents scale as a function of lander mass (or thrust).
7) Images taken with varying incidence and emission angles reveal that HR-BZs are less backscattering than the undisturbed regolith.

References

[1] Hapke, B., and H. Van Horn, (1963), *JGR*, *68*, 4545. [2] Kaydash V. et al. (2011), *Icarus*, *211*, 89-96. [3] Clegg R. N. and Jolliff B. L. (2012), *LPSC XLIII*, Abstract #2030. [4] Hapke B.W. (1981), *JGR*, *86*, 3039-3054. [5] Carrier W.D. (1991), *Lunar Sourcebook*, 475-594. [6] Hapke B. W. (2001), *Icarus*, *167*, 523-524. [7] Hapke B. W. et al. (2012), *JGR*, *117*. [8] Goguen J.D. et al. (2010), *Icarus*, *208*, 548-557. [9] Lucey, P. et al. (2006), *New Views of the Moon*, 84-219. [10] Graf J. (1993), *Lunar Soils Grain Size Catalog*. [11] Morris R. V. et al. (1983), *Handbook of Lunar Soils*. [12] Blanchard, D. P. et al. (1977), *LPI Conference on Luna 24*. [13] Laul, J. C.,and Schmitt E. A. (1973), *GCA*, *37*, 927-942. [14] Kaydash V. G. and Shkuratov Y. G. (2012), *SSR*, *46*, 108-118. [15] Metzger, P. et al. (2011), *JGR*, *116*, E06005. [16] Immer, et al. (2011), *Icarus*, *211*, 1089–1102. [17] Metzger, P. et al. (2010), *Lunar Settlements*, 551-576. [18] Shkuratov Y. et al. (2012), *PSS*.

Acknowledgements

We thank NASA for support of the LRO mission and the LROC Operations Team for making available the data used in this research.